Organic Geochemistry 40 (2009) 353–364

Contents lists available at ScienceDirect

Organic Geochemistry

journal homepage: www.elsevier.com/locate/orggeochem

Characterization of permineralized kerogen from an Eocene fossil fern

Andrew D. Czaja [a,*], Anatoliy B. Kudryavtsev [b], George D. Cody [c], J. William Schopf [d]

[a] Department of Earth and Space Sciences, Center for the Study of Evolution and the Origin of Life, Institute of Geophysics and Planetary Physics, University of California, Los Angeles, CA 90095-1567, USA
[b] Center for the Study of Evolution and the Origin of Life, Institute of Geophysics and Planetary Physics, and NASA Astrobiology Institute, University of California, Los Angeles, CA 90095-1567, USA
[c] Geophysical Laboratory, Carnegie Institution of Washington, 5251 Broad Branch Road NW, Washington, DC 20015, USA
[d] Department of Earth and Space Sciences, Center for the Study of Evolution and the Origin of Life, Institute of Geophysics and Planetary Physics, Molecular Biology Institute and NASA Astrobiology Institute, University of California, Los Angeles, CA 90095-1570, USA

ARTICLE INFO

Article history:
Received 14 August 2007
Received in revised form 1 December 2008
Accepted 2 December 2008
Available online 10 December 2008

ABSTRACT

The processes of organic maturation that occur during the permineralization of fossils and the detailed chemistry of the resulting products are incompletely understood. Primary among such processes is the geochemical alteration of biological matter to produce kerogen, such as that which comprises the cell walls of the fossils studied here: essentially unmetamorphosed, Eocene plant axes (specimens of the fossil fern *Dennstaedtiopsis aerenchymata* cellularly permineralized in cherts of the Clarno Formation of Oregon and the Allenby Formation of British Columbia). The composition and molecular structure of the kerogen that comprises the cell walls of such axes were analyzed using ultraviolet Raman spectroscopy (UV–Raman), solid state ^{13}C nuclear magnetic resonance spectroscopy (^{13}C NMR) and pyrolysis–gas chromatography–mass spectrometry (py–GC–MS).

Cellularly well-preserved fern axes from both geologic units exhibit similar overall molecular structure, being composed primarily of networks of aromatic rings and polyene chains that, unlike more mature kerogens, lack large polycyclic aromatic hydrocarbon (PAH) constituents. The cell walls of the Allenby Formation specimens are, however, less altered than those of the Clarno chert, exhibiting more prevalent oxygen-containing and alkyl functional groups and comprising a greater fraction of rock mass.

The study represents the first demonstration of the effectiveness (and limitations) of the combined use of UV–Raman, ^{13}C NMR and py–GC–MS for the analysis of the kerogenous cell walls of chert-permineralized vascular plants.

1. Introduction

The processes of organic maturation that occur during fossilization and subsequent preservation are incompletely defined, primarily because the geologic timeframe of fossil formation and accompanying geochemical alteration cannot be replicated in a controlled laboratory setting. However, recent confined pyrolysis experiments, performed in an attempt to mimic such alteration, have been somewhat successful, especially in understanding the composition of fossil plants, arthropods and associated kerogen (e.g., Stankiewicz et al., 2000; Gupta et al., 2006c, 2007c). In nature, fossilization and organic maturation occur over long durations and an understanding of the conditions (of temperature, pressure, mineralogy, associated fluid chemistry, etc.) that existed in and around a given fossil-bearing rock unit during the millions to billions of years after rock formation is necessarily incomplete. The chemistry of the kerogen (a complex material composed of particulate carbonaceous matter insoluble in organic solvents) formed during such processes is also incompletely understood, a deficiency that reflects the variability and complexity of its structure, current knowledge of which, including a history of its study, is presented in a recent review by Vandenbroucke and Largeau (2007).

The geochemical alteration of organic matter (OM) and the diagenetic production of kerogen have been extensively studied. A primary focus of such work has been the formation of coal, oil and natural gas (e.g., Ishiwatari et al., 1976, 1977; Peters et al., 1977; Tissot and Welte, 1984; Hatcher et al., 1988; de Leeuw and Largeau, 1993; Greenwood et al., 1993, 2001; Hunt, 1996), whereas other studies have focused on more intense levels of the geochemical alteration of OM, including the graphitization that occurs during metamorphism (e.g., Pasteris and Wopenka, 1991; Wopenka and Pasteris, 1993; Yui et al., 1996; Beyssac et al., 2002). Other studies have provided new insights into kerogen formation and the origins of sedimentary aliphatic materials (Tegelaar et al., 1989; de Leeuw and Largeau, 1993; Briggs, 1999; Gupta et al.,

* Corresponding author. Present address: University of Wisconsin–Madison, Department of Geology and Geophysics, Madison, WI 53706, USA. Tel.: +1 608 262 4255; fax: +1 608 262 0693.
E-mail address: aczaja@geology.wisc.edu (A.D. Czaja).

0146-6380/$ - see front matter © 2008 Elsevier Ltd. All rights reserved.
doi:10.1016/j.orggeochem.2008.12.002

2006b, 2007a,b,d). In general, either coal or particulate kerogen have been analyzed in such studies. Among the exceptions are studies of the OM that comprises fossil graptolites (Bustin et al., 1989; Gupta et al., 2006a), palynomorphs (Yule et al., 1998, 2000; Bernard et al., 2007), conodonts (Marshall et al., 2001), cephalopod jaws (Gupta et al., 2008a) and fish scales (Gupta et al., 2008b). Only recently has the thermal history of kerogen in fossils preserved via permineralization been studied (Kudryavtsev et al., 2001; Schopf et al., 2002, 2005). The present work extends such studies by combining the use of UV–Raman spectroscopy, solid state ^{13}C nuclear magnetic resonance spectroscopy (^{13}C NMR), and pyrolysis–gas chromatography–mass spectrometry (py–GC–MS) for the analysis of such kerogens.

Though an analytical tool used widely in geochemistry and other branches of science and technology, Raman spectroscopy is still relatively new to paleobiology. Recently, however, it and the more advanced technique of Raman imagery have been used to analyze the structural composition and kerogenous cellular make-up of morphologically preserved fossils (Roberts et al., 1995; Schweitzer et al., 1997; Arouri et al., 2000; Dietrich et al., 2001; Kudryavtsev et al., 2001; Marshall et al., 2001, 2005a; Nestler et al., 2003; Schopf and Kudryavtsev, 2005; Schopf et al., 2005, 2008; Bernard et al., 2007; Chen et al., 2007; Jacob et al., 2007), including some of the oldest putative fossils known, microbe-like filaments permineralized in the ca. 3465 Ma Apex chert (Schopf et al., 2002, 2007), the ca. 3490 Ma Dresser Formation (Ueno et al., 2001; Schopf et al., 2007), the ca. 3200 Ma Dixon Island Formation (Kiyokawa et al., 2006), the ca. 2970 Ma Farrel Quartzite (Sugitani et al., 2007), all from northwestern Western Australia, and the >2440 Ma Harris Greenstone Domain (Zang, 2007) of South Australia. Additionally, Raman spectroscopy has been used to analyze OM preserved in the ca. 3430 Ma Strelley Pool Chert (Allwood et al., 2006; Marshall et al., 2007), also from northwestern Western Australia, as well as apatite-hosted graphitic inclusions in ca. 3830 Ma metasediments of southwestern Greenland, possibly the oldest evidence of life on Earth (McKeegan et al., 2007). In contrast to these studies, the work described here was performed, in part, by using UV–Raman rather than VIS–Raman spectroscopy. Vibrational excitation of very immature kerogens (such as here) using either ultraviolet or visible laser light produces visible wavelength fluorescence, a response that masks the relatively weak Raman signal in VIS– but not UV–Raman spectra.

Solid state ^{13}C NMR has been used to investigate many carbonaceous materials, including preserved OM such as that in coals (e.g., Snape et al., 1979), fossil spores (e.g., Hemsley et al., 1995, 1996) and fossil leaves (van Bergen et al., 1994b; Lyons et al., 1995; Briggs, 1999; Almendros et al., 2005; Gupta et al., 2007c). Similarly, py–GC–MS has been used extensively to analyze the organic components of fossil plants and other kerogenous materials (e.g., Hatcher et al., 1988; Faix et al., 1990; Rullkötter and Michaelis, 1990; Ralph and Hatfield, 1991; Greenwood et al., 1993; van Bergen et al., 1994a,b, 1997; Lyons et al., 1995; Stankiewicz et al., 1996, 1997, 1998, 2000; Briggs et al., 1998; Briggs, 1999; Marshall et al., 2005b; Gupta et al., 2006a,b, 2007a,b,c,d, 2008a,b; Boyce et al., 2007; Dutta et al., 2007; Jacob et al., 2007).

We show here that UV–Raman, ^{13}C NMR and py–GC–MS can provide mutually reinforcing lines of data regarding the geochemical characteristics of the carbonaceous matter that comprises fossil plants. In a given fossil plant specimen, Raman spectroscopy can provide information about the molecular structure of its kerogenous constituents; ^{13}C NMR can provide additional information about such molecular structure, as well as evidence of the types and quantities of carbon moieties present (aromatic, aliphatic, etc.); py–GC–MS can yield important insight into the nature and composition of the fossilized OM. Of the three techniques, only UV–Raman is non-invasive and non-destructive and can be used to investigate samples on a much finer spatial scale (ca. 1 μm) than ^{13}C NMR and py–GC–MS, both of which require small (ca. 100 mg and ca. 100 μg, respectively) bulk samples [a technique called laser–micropyrolysis–GC–MS can be used to analyze carbonaceous materials on a finer spatial scale than standard py–GC–MS, but is also destructive and spot sizes are typically ca. 50–400 μm (Greenwood et al., 1996, 2002)]. However, UV–Raman cannot provide complete information about the molecular structure of kerogens such as those discussed herein. When vibrationally excited by monochromatic ultraviolet laser light (such as the 244 nm wavelength used here), certain structures (e.g., aromatic rings and conjugated C=C bonds) in such kerogens produce Raman spectral bands that are increased in intensity by orders of magnitude (Barańska et al., 1987) because of resonance enhancement. Such enhancement can "swamp out" other spectral bands (e.g., those from saturated hydrocarbons, a typical component of immature kerogens such as those discussed herein) that are not enhanced. The combined use of ^{13}C NMR and py–GC–MS, together with UV–Raman, provides a means of assessing the effects of such enhancement.

The present study compares the relative degrees of preservation of fossilized fern axes of a single taxon permineralized in cherts of two Eocene geologic units. The analyses were designed to determine the structure and composition of the cellularly preserved kerogen of the fossils in each unit (including any original biomolecules or recognizable biomolecular fragments). All of the fossil fern axes would have originally been composed of identical materials, primarily cellulose (the main component of plant cell walls) and lignin (the primary structural biomolecule in the cell walls of certain types of plant tissues). Despite such biomolecular similarity, the fossilized products preserved in the two units need not be identical: local biologic, geologic and geochemical conditions also play important roles in determining the nature of the OM preserved in such fossils. Though the complete history of such conditions cannot be known precisely, variability between fossils of a single taxon that are as similarly preserved as the specimens here can most plausibly be assumed to reflect (i) differing thermal/geologic histories after permineralization (e.g., fossils of one formation having been exposed to higher temperature and/or pressure); and/or (ii) taphonomic differences prior to permineralization (e.g., resulting from differing rates of microbial degradation during rapid vs. slow burial). We have analyzed kerogens of fern rhizomes preserved in the two geologic units in order to address possible differences in chemistry arising from both sources.

This study, the first recorded use of UV–Raman spectroscopy for the analysis of permineralized cellular fossils, documents the compositional and structural similarities and differences between the various specimens. It also well illustrates the usefulness of UV–Raman as a complement to other analytical techniques (viz. ^{13}C NMR and py–GC–MS) that have been typically used in such studies.

2. Materials and methods

2.1. Fossil ferns

The fossil fern here studied is *Dennstaedtiopsis aerenchymata* (Fig. 1). Cherts containing three dimensionally preserved fossil fern rhizomes (subterranean stems; Fig. 1a and b) of this taxon were collected from two Eocene geologic units: the Clarno Formation of north-central Oregon, USA (Arnold and Daugherty, 1964; Fig. 1f), acquired from the Precambrian Paleobiology Research Group (PPRG) collection at the University of California, Los Angeles (sample #456; Walter et al., 1983); and the Princeton chert of the Allenby Formation of British Columbia, Canada (Miller, 1973; Fig. 1f), acquired from the University of Alberta Paleobotanical Collection (UAPC-ALTA; specimens on permanent loan to J.W.S.). The

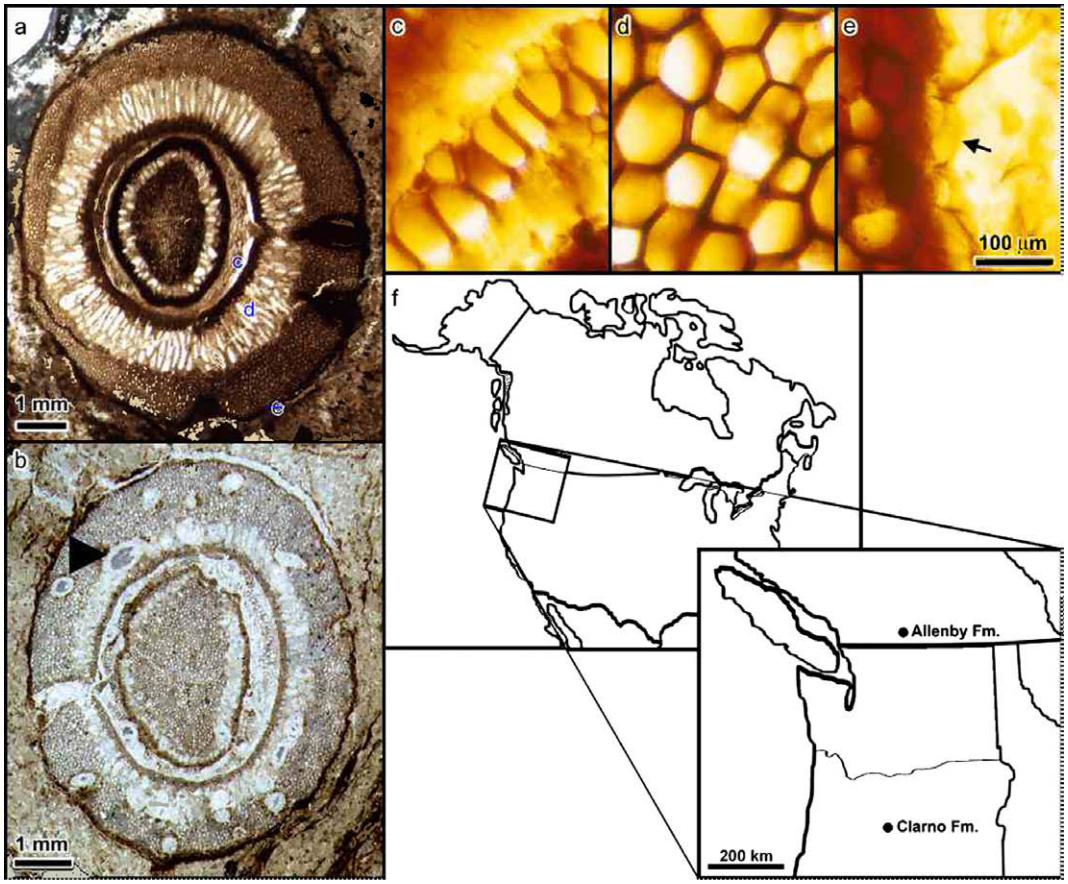

Fig. 1. Optical photomicrographs showing transverse sections of chert-permineralized rhizomes of the fossil fern *Dennstaedtiopsis aerenchymata* (a–e) and the geographic locations from which samples were collected (f). (a) Rhizome from Clarno chert in petrographic thin section (transmitted light). (b) Rhizome from Princeton chert in cellulose acetate peel (reflected light) in which the large arrowhead points to an example of the fungal hyphae typically preserved in the cortical and vascular tissues of such specimens. Xylem (c), cortical (d) and epidermal cells (e) of a Clarno chert rhizome (transmitted light); the scale in (e) applies also to (c) and (d). The locations within such rhizomes of the three cell types illustrated are indicated by the corresponding letters in (a).

localities of the Clarno and Princeton cherts from which the fossils were collected are described, respectively, by Walter et al. (1983) and Miller (1973) and the descriptions are summarized in Table 1.

2.2. Model compounds

To aid in the assignment of the UV–Raman spectral bands from the fossil ferns, model compounds that contain portions of the proposed structure of their kerogen were also analyzed. These included enzyme lignin (USDA Forest Products Laboratory, Madison, WI); β-carotene, 1,4-bis(2-methylstyryl)benzene, 2,4-hexadiene and 2-butene-1,4-diol (Sigma–Aldrich, Inc., St. Louis, MO); benzene (Burdick and Jackson Laboratories, Inc., Muskegon, MI); xylene (Fisher Scientific, Fairlawn, NJ); and graphite (highly ordered, pyrolytic graphite, HOPG SPI–3; Structure Probe, Inc., West Chester, PA).

2.3. Sample preparation

Two types of samples were prepared: (1) ca. 150 µm thick petrographic thin sections, used for Raman spectroscopic in situ anal-

Table 1
Geological settings of fossil samples.

	Clarno chert[a]	Princeton chert[b]
Stratigraphy	Clarno Formation	Allenby Formation
Tectonic unit/ location	Clarno Fm., John Day Basin, north-central Oregon, USA	Princeton Basin, Princeton Grp., British Columbia, Canada
Geologic age	Eocene	Middle Eocene (~49 Ma; based on fish and mammal fossils and K–Ar dating)
Paleoenvironment	Megafossiliferous, carbonaceous cherts (a silicified peat bog) accumulated in a terrigenous basin associated with volcaniclastics	Megafossiliferous (including aquatic plants, fish, reptiles, mammals), carbonaceous chert accumulated in shallow/near shore, soft bottom lake deposit[c]
Metamorphic grade	Apparently unmetamorphosed	Apparently unmetamorphosed
Locality	J.W.S. "Perret Ranch Locality" of 1972 (H.J. Perret Ranch about 10 km northeast of Redmond, central Oregon)	Princeton chert outcrop, east side of Similkameen River, ~8.4 km south of Princeton, British Columbia, near abandoned mining town of Allenby
Description	Black, carbonaceous chert, containing numerous axes of fossil vascular plants	Alternating layers of black to gray chert and coal containing occasional ash beds

[a] Walter et al. (1983).
[b] Smith and Stockey (2003).
[c] Cevallos-Ferriz et al. (1991).

ysis of individual fossil cell walls (see Fig. 1c–e); and (2) HF-macerated kerogenous residues of individual fossils that were analyzed using ^{13}C NMR and py–GC–MS. The thin sections were prepared using standard techniques, mounted onto glass microscope slides by use of acetone-soluble cement, and the contained fern axes were located and documented using optical microscopy/photomicrography (Fig. 1). The fossil-bearing chert slices were then removed from their glass slides by dissolution of the cement and cleaned for 10 h in a Soxhlet extractor using a solution of benzene and MeOH (1:1 v/v; cf. Schopf et al., 2005).

Standard (palynological) acid maceration techniques (e.g., Wellman and Axe, 1999) were modified slightly. Prior to maceration, individual fossil fern rhizomes were cut away from the surrounding matrix by use of a thin-bladed rock saw, making it possible to prepare kerogen samples of the axes rather than of the bulk chert. The axes from each geologic unit thus isolated were divided into replicate sets, cleaned using a Soxhlet extractor as described above (typically for 24 h) and rinsed thoroughly with deionized water. The samples were then macerated in ca. 25% HF. The resulting kerogenous residues were rinsed several times with deionized water to remove excess acid and dried in a desiccant-containing vacuum chamber.

Each sample was evaluated in terms of its kerogen abundance by comparing its dry mass of macerated kerogen to the mass of the permineralized axes prior to dissolution in acid (in mg g^{-1}; see Fig. 2). Thus, the kerogen abundances (Fig. 2) represent only the preserved OM of the fossil fern axes and not the bulk chert which include diffuse organic detritus from various sources.

2.4. Analytical techniques

UV–Raman analysis was performed by use of the JY Horiba T64000 triple-stage VIS–/UV–Raman system described by Schopf and Kudryavtsev (2005). An excitation wavelength of 244 nm was provided by a Coherent Innova 90C FreD frequency doubling argon ion laser. To avoid excessive sample heating and ensure that the spectra reported did not reflect chemical alteration by the impinging laser beam, the fossil-bearing rock slices and powdered model compounds were placed on UV-transparent fused quartz microscope slides, the liquid model compounds were analyzed in square sided quartz vials and various laser powers were tested. The optimum power for in situ analysis of the fossil ferns and their encompassing chert matrices was found experimentally to be ca. 12 mW (calculated to be ca. 0.5 mW at the sample surface). Use of this and lower laser power produced virtually identical band patterns from, and no visible damage to, the specimens. Higher laser power produced a slight broadening and a change in the relative intensities of the first-order bands in the spectra. Similar tests were performed to determine the optimum laser power for analysis of the model compounds and were found to be ca. 1 mW (ca. 0.04 mW at the sample) for powders [enzyme lignin, β-carotene and 1,4-bis(2-methylstyrl)benzene] and ca. 100 mW (ca. 4 mW at the sample) for liquids (benzene, xylene, 2,4-hexadiene and 2-butene-1,4-diol) and the graphite standard.

Areas in each sample were located and positioned for UV–Raman analysis by use of an Olympus BX41 microscope equipped with a 40 × UV objective (NA = 0.50; OFR Inc., Caldwell, NJ) and a motorized high precision stage (SCAN 75 × 50, Märzhäuser GmbH & Co., KG, Wetzlar-Steindorf, Germany). The optics enabled the laser to be focused to a spot size of ca. 2–3 μm. The spectra for the fossil ferns represent averages of point spectra collected from multiple positions along a cell wall with each such point spectrum representing the average of two 1 s measurements. This procedure, providing an acceptable signal/noise ratio while ensuring that the fossil ferns were not chemically or physically altered during analysis, is similar to that detailed by Czaja et al. (2006). The powdered

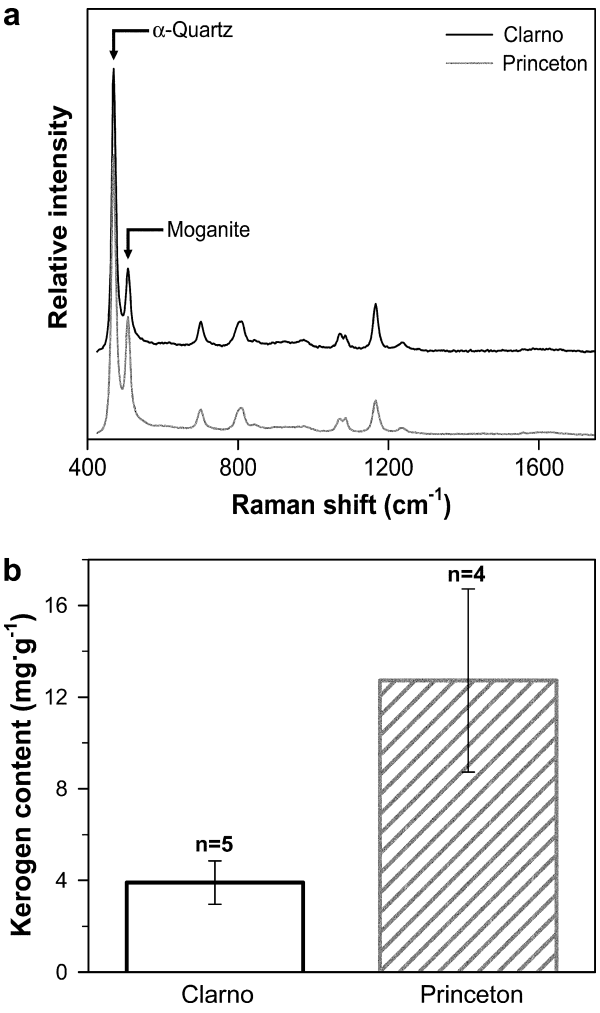

Fig. 2. Raman spectra and kerogen content of Clarno and Princeton cherts. (a) Representative UV–Raman spectra of the chert matrices of the two geologic units; all peaks in the region from 425 to 1260 cm^{-1} represent vibrational modes of silica. (b) Amounts of kerogen macerated from fossil fern rhizomes of the two units (mg g^{-1} = dry weight of kerogen recovered from the axes divided by the weight of the axes before maceration; n = number of samples; error bars are ±1 standard deviation).

model compounds were analyzed with techniques essentially identical to those used for the fern axes, whereas spectra of the liquid model compounds and those of the quartz matrices of the fossil ferns were acquired from single rather than multiple points.

Solid state, variable amplitude CP–MAS (cross-polarization, magic angle spinning) ^{13}C NMR analysis was performed by use of a Varian-Chemagnetics Infinity solid state spectrometer. The fossil fern kerogen samples, ranging from ca. 25 to 100 mg, were packed into standard NMR tubes and spun at the magic angle (54.7°) at 11.5 kHz within a magnetic field of static strength 7.05 T. ^{13}C NMR spectra were acquired using a proton excitation pulse ($\pi/2$) of 4.0 μs, a contact time of 4.5 ms and a decoupling power ($\omega_I/2\pi$) of 75 kHz. The spectra were referenced to hexamethyl benzene (a secondary reference) and are reported in ppm relative to the methyl group in tetramethylsilane. The system is described by Cody et al. (2002).

Py–GC–MS analyses were performed by use of a Hewlett-Packard 6890 series gas chromatograph having a 50% phenyl-polydimethoxysilicon column interfaced to an HP 5972 quadrupole mass spectrometer. The GC oven temperature program was 50–300 °C at 5 °C min^{-1}. Pyrolysis of ca. 100 μg of each of the fossil samples was performed using a CDS 1000 pyroprobe attached

to the injector port of the gas chromatograph (injector held at 300 °C). The pyrolysis heating rate was 500 °C s^{-1} to 610 °C (held 10 s). The pyrolysate was introduced to the GC column by use of He as carrier gas. The system is described in detail by Wang et al. (2005). The resulting spectra were analyzed and their constituent peaks identified by use of library mass spectra and published data (Hatcher et al., 1988; Pouwels et al., 1989; Ralph and Hatfield, 1991; Greenwood et al., 1993, 2001). The data are presented as ratios of the area of each individual peak to those of the total ion chromatograms expressed as percentages. The peaks were not normalized by use of response factors but, because all spectra were measured using the same equipment and analytical settings, the intensity of each pyrolysis product of each kerogen sample is comparable to that of the corresponding pyrolysis product of all other samples.

2.5. Spectral deconvolution

Deconvolution of the ^{13}C NMR and UV–Raman spectra bands was accomplished by use of the spectral analysis program PeakFit version 4.12 (Seasolve Software, Inc., San Jose, CA). ^{13}C NMR spectra were fitted with bands described by Gaussian mathematical functions and UV–Raman spectra with those described by a mixture of Gaussian and Lorentzian mathematical functions. For each deconvoluted spectrum, the quality of fit of the bands was assessed using the statistical criteria discussed by Schopf et al. (2005).

3. Results and discussion

3.1. Clarno and Princeton cherts

The Clarno and Princeton chert specimens are mineralogically quite similar, being composed of multiphase microcrystalline quartz. UV–Raman spectra acquired from organic-poor regions of the cherts exhibit two main bands (Fig. 2a), an intense band centered at ca. 465 cm^{-1}, attributable to α-quartz (the most common phase of quartz) and a second band centered at ca. 500 cm^{-1}, attributable to moganite, a polymorph of microcrystalline silica (Kingma and Hemley, 1994). The relative intensities of these bands were somewhat variable in the UV–Raman spectra, evidencing heterogeneity in the distribution and abundance of the two dominant quartz phases.

Despite such similarity, the specimens of the cherts exhibit notable differences. In hand specimens, the Clarno chert is relatively homogeneous both in texture and color, being predominately glassy and very dark brown to black. In contrast, the Princeton chert is less glassy, composed of relatively well defined mm to cm thick organic-rich layers. The two cherts also differ substantially in the amount of preserved OM, as demonstrated by the kerogen content of plant axes from the two units. The amount of kerogen in the rhizomes of each unit is similar, but the average kerogen content of those of the Clarno chert is only about one third that of the Princeton chert axes (Fig. 2b). This difference suggests that the OM of the Clarno chert may be less well preserved, i.e. more geochemically altered, than that of the Princeton chert.

3.2. Fossil fern kerogen of Clarno and Princeton cherts

The data indicate that the fossil ferns are composed predominantly of aromatic hydrocarbons, both single ring and small PAHs, that exhibit a substantial amount of alkyl- and oxygen-substitution. These aromatic rings and PAHs are interlinked by polyene chains (aliphatic chains with multiple alternating single and double bonds) as well as other alkyl groups and oxygen bridges. This interpretation, consistent with previous analyses of other well preserved fossil plants (e.g., Behar and Vandenbroucke, 1987; Rullkötter and Michaelis, 1990; Boyce et al., 2002, 2003) is based on the several lines of evidence considered below. In the sections that follow, the kerogen of the Clarno chert rhizomes is addressed first, followed by a discussion of the similarities and differences between the kerogen composition and molecular structure of fossil axes of each unit.

3.2.1. Clarno chert fossil fern rhizomes

Although the macromolecular composition of the kerogen of the Clarno chert fern rhizomes, measured from py–GC–MS, is rather complex (Fig. 3, upper spectrum), the products can be grouped into a small number of classes (Table 2). Small alkyl-substituted aromatic molecules and small oxygen-substituted aromatic molecules together comprise a majority of the pyrolysate (ca. 50% and ca. 25%, respectively). Small PAHs (mostly naphthalene or alkyl-substituted naphthalenes) make up a much smaller proportion (ca. 7%). The other major category of carbonaceous material detected is aliphatic carbon (mainly as *n*-alkanes; Table 2), which comprises ca. 15% of the pyrolysate.

No evidence of the presence of assured derivates of lignin (guaiacyl units: *m/z* 124 + 138 + 150 + 164; syringyl units: *m/z* 154 + 168 + 180 + 194) or cellulose (levoglucosan: *m/z* 60 + 93) was detected from py–GC–MS (cf. Hatcher et al., 1988; Pouwels et al., 1989; Ralph and Hatfield, 1991; Pastorova et al., 1994). Though lignin contains substantial amounts of oxygen-substituted aromatic moieties, the phenolic pyrolysis products of the fossil ferns (Table 2) are too simple to be firmly diagnostic of lignin. Due to the hydrolysis of its glycosidic bonds, cellulose is degraded more rapidly than lignin in acidic peat deposits such as those represented by the cherts here (Hatcher et al., 1988), so absence is not unexpected. The abundance of phenols in the pyrolysates of the fossil ferns and the lack of any detectable assured derivatives of lignin and cellulose indicate that the kerogen comprising these essentially unmetamorphosed plant axes has been appreciably altered, transformed from the original biochemical composition to geopolymers similar to those of an intermediate rank coal (Axelson, 1985; Hatcher et al., 1988).

^{13}C NMR analysis further supports the interpretation of the nature of the kerogen comprising the Clarno fossil rhizomes. Deconvolution of the spectra indicates that each is comprised of 14 constituent bands (Fig. 4). The bands are attributed to various types of aliphatic and aromatic carbon (bands centered between 0 and 50 ppm and between 100 and 155 ppm, respectively), as well as to carboxyl (those centered between 165 and 175 ppm) and carbonyl carbon (that centered at 205 ppm). A low-intensity band at ca. 75 ppm (Fig. 4), not attributed to a specific carbon moiety, is present in the "saddle" between the sets of aromatic and aliphatic bands. Bands at this position have been attributed to the secondary alcohols of polysaccharides ($R–CH_2–OH$; VanderHart and Atalla, 1984; Gil and Neto, 1999) including cellulose, the most abundant polysaccharide in plants. However, as noted above, py–GC–MS analysis revealed no evidence of cellulose or its derivatives in any of the fossil fern kerogen samples analyzed. Bands at ca. 75 ppm have also been attributed to the alkyl carbons of alkyl-aryl ether linkages (i.e. $R–CH_2–O–C_{ar}$) in lignin (Leary and Newman, 1992) and to those in kerogen derived from lignin-rich material (Cody and Sághi-Szabó, 1999).

The cell walls of three tissues (xylem, cortex and epidermis; Fig. 1c–e) of the Clarno and Princeton chert fossil fern axes were analyzed by use of UV–Raman spectroscopy. In living ferns, the main difference between the cell walls in such tissues measurable using UV–Raman is the relative abundance of cellulose and lignin (Czaja, 2006). In the fossils analyzed here, however, the cellulose originally present has been geochemically degraded. Not surprisingly, therefore, no apparent differences were detected in the

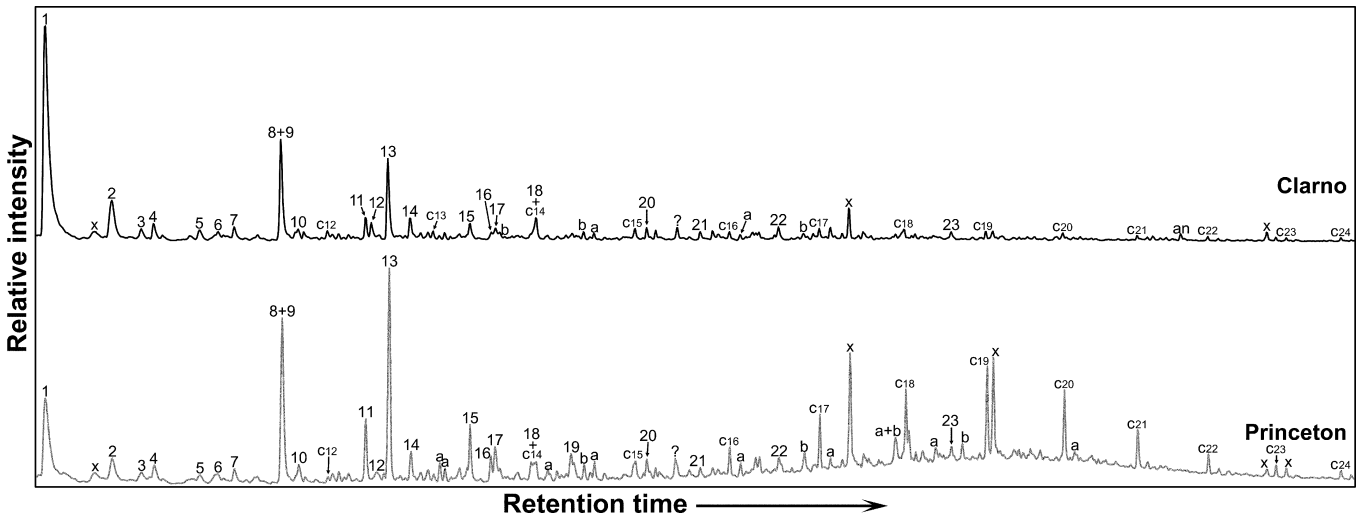

Fig. 3. Representative py–GC–MS total ion chromatograms of fossil fern kerogens from the Clarno and Princeton cherts; x, analytical contaminant; ?, undetermined component; all other components are identified by peak labels in Table 2.

Table 2
Major pyrolysis products of kerogen macerated from fossil fern rhizomes of Clarno and Princeton cherts.

Component[a]	Av. % of total[b]					
	Class	Clarno	s.d.[c]	Princeton	s.d.	Peak label[d]
Toluene	Ar[e]	37.7	4.2	13.3	2.6	1
Xylene	Ar	7.3	0.1	3.8	0.6	2, 3
Styrene	Ar	1.8	0.3	1.9	0.6	4
Ethylmethyl- and trimethylbenzene	Ar	2.4	0.3	1.7	0.3	5, 7
2-Methyl-2-cyclopenten-1-one	K_c[f]	1.1	0.1	0.7	0.2	6
Phenol + benzaldehyde	C_{ar}–O[g]	10.5	2.1	12.6	2.5	8 + 9
Benzofuran	C_{ar}–O	0.8	0.1	1.6	0.5	10
Methylphenol	C_{ar}–O	6.8	2.1	9.9	4.7	11, 13
2,3-Dimethylcyclopent-2-en-1-one	K_c	0.9	0.2	<0.5	–	12
Acetophenone	C_{ar}–O	1.6	0.0	1.7	0.3	14
Dimethylphenol	C_{ar}–O	1.9	0.5	2.6	1.3	15, 16
Ethylphenol	C_{ar}–O	<0.5	–	0.9	0.8	17
Naphthalene	PAH[h]	2.4	1.4	1.5	1.2	18
Ethylmethylphenol	C_{ar}–O	<0.5	–	1.3	0.8	19
Methylnaphthalene	PAH	1.9	0.5	1.3	0.1	20
2,3-Dihydro-1H-inden-1-one	C_{ar}–O	0.5	0.1	<0.5	–	21
Dimethylnaphthalene	PAH	1.4	0.7	0.8	0.1	22
Trimethylnaphthalene	PAH	0.9	0.1	1.3	0.5	23
n-Alkanes	Al[i]	7.7	1.9	21.2	3.9	Cn[j]
n-Alkenes	Al	2.2	0.0	3.7	0.6	a
Branched alkanes	Al	2.0	0.2	3.0	0.5	b

[a] Pyrolysis products averaging 0.5% or more of total peak area for kerogen from each unit.
[b] Average of % of total measured peaks for kerogen from each unit (Clarno, $n = 2$; Princeton, $n = 3$).
[c] 1 standard deviation.
[d] Peak labels refer to those in Fig. 4.
[e] Alkyl-substituted aromatic carbon.
[f] Cyclic ketones.
[g] Oxygen-substituted aromatic carbon.
[h] Polycyclic aromatic hydrocarbons.
[i] Aliphatic carbon.
[j] Number of carbons in each alkane.

molecular structure of the various fossilized tissues analyzed using UV–Raman. Consequently, the structure of the xylem cell wall kerogen detailed below is representative of that of all of the tissues of the fossil ferns studied.

The UV–Raman spectra of the fossils are composed of two main groups of bands: those between 2500 and 3300 cm^{-1} and those between 1100 and 1800 cm^{-1} (Fig. 5). The broad, low intensity features in the 2500–3300 cm^{-1} region closely resemble bands in the spectra of well preserved, permineralized fossil microorganisms (Schopf et al., 2005) as well as those of other carbonaceous materials (Ferrari and Robertson, 2001; Jackson et al., 2003). Like previous workers, we interpret these bands to represent second-order vibrational modes of bands in the 1100–1800 cm^{-1} region and/or aromatic and aliphatic C–H stretching modes (the latter being functionalities known to be present on the basis of py–GC–MS and ^{13}C NMR). Because these broad, low-intensity bands are essentially identical in all the spectra from the fossil fern axes, they are not considered further. The following discussion therefore focuses only on the first-order bands of the fossil kerogens, those between 1100 and 1800 cm^{-1}.

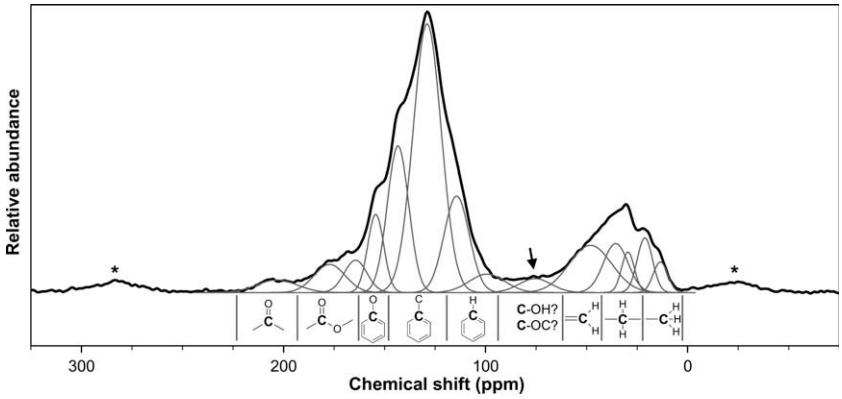

Fig. 4. Representative ^{13}C NMR spectrum of fossil fern kerogen from Clarno chert (thick black line) and results of its deconvolution (gray lines); asterisks denote spinning side bands of the main aromatic carbon band at ca. 130 ppm. The constituent peaks determined by deconvolution are present in the spectra of all of the kerogens studied, though in slightly differing proportions. The band assignments indicated by the structures illustrated below the spectra are based on those of Snape et al. (1979), Axelson (1985) and Cody et al. (2002).

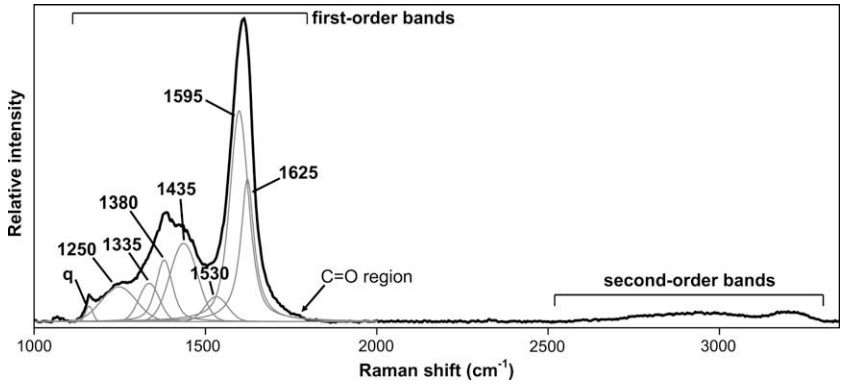

Fig. 5. Representative UV–Raman spectrum of a Clarno chert fern xylem cell wall analyzed in petrographic thin section (thick black line); "q" denotes principle quartz band of the chert matrix in this region (compare with spectra in Fig. 2a). Gray lines show results of deconvolution of the first-order bands of the spectrum.

The first-order region of the Clarno fern cell wall UV–Raman spectra is composed of eight bands (Fig. 5) that can be divided into two sets, those between 1500 and 1800 cm^{-1} and those between 1100 and 1500 cm^{-1}. Though superficially similar to the "G-band" and "D-band", respectively, of the first-order region of VIS–Raman spectra of kerogens and other carbonaceous materials (e.g., Wopenka and Pasteris, 1993; Yui et al., 1996; Jehlička and Beny, 1999; Kudryavtsev et al., 2001; Beyssac et al., 2002; Schopf et al., 2002, 2005), these UV–Raman spectral features are not attributed solely to the molecular structures documented by earlier VIS–Raman work. In such studies, the G-band has been ascribed to the synchronous ring stretching vibration of PAHs and the D-band to modes of aromatic ring-deformation and totally symmetric breathing (Mapelli et al., 1999; Ferrari and Robertson, 2001; Schopf et al., 2005). Unlike the kerogens in such earlier work, those here are composed predominantly of small aromatic moieties and PAHs, as documented above, and the use here of UV– rather than of VIS–Raman results in resonant enhancement of bands in the "G" and "D" regions that are derived from different structural features than those identified by previous studies.

We interpret the UV–Raman spectra of the fossil ferns to indicate the presence of both polyene chains and PAHs. The spectra (e.g., Figs. 5 and 6a) are similar to those of other organic materials such as lignin (Fig. 6b and Halttunen et al., 2001), β-carotene (Fig. 6c and Saito et al., 1983) and certain types of amorphous sp^2/sp^3-bonded carbonaceous matter (Li and Stair, 1997a,b; Gilkes et al., 1998; Ferrari and Robertson, 2001; Chua and Stair, 2003; Jackson et al., 2003). Despite the obvious molecular differences among these materials and the fact that previous UV–Raman analyses of small PAHs (Asher, 1984, 1993; Asher and Johnson, 1984; Chua and Stair, 2003) indicate that some vibrational modes of such molecules produce bands in the ca. 1600 and ca. 1400 cm^{-1} regions, the similarity of the Raman spectra of such materials strongly suggests that they share distinctive molecular structures, in particular carbon rings interlinked by polyene chains. However, as shown by the deconvoluted fossil fern spectrum in Fig. 5, the band at ca. 1600 cm^{-1} is composed of two constituent bands and is not identical to those in the spectra of lignin and β-carotene (Fig. 6b and c).

That the UV–Raman spectral bands in question are due to vibrational modes of polyene chains as well as to those of PAH moieties is supported by earlier Raman studies of carbonaceous materials. In particular, the kerogens of permineralized fossils of various geologic ages and degrees of preservation analyzed using VIS–Raman have also been interpreted to be, in part, composed of polyene chains (Schopf et al., 2005). Additionally, amorphous carbonaceous materials produced by the extreme compression of benzene, as analyzed using UV–Raman, exhibit spectral patterns similar to those of the fossil rhizomes here and have been interpreted to be composed of benzene rings and small PAHs interlinked by polyene chains (Jackson et al., 2003).

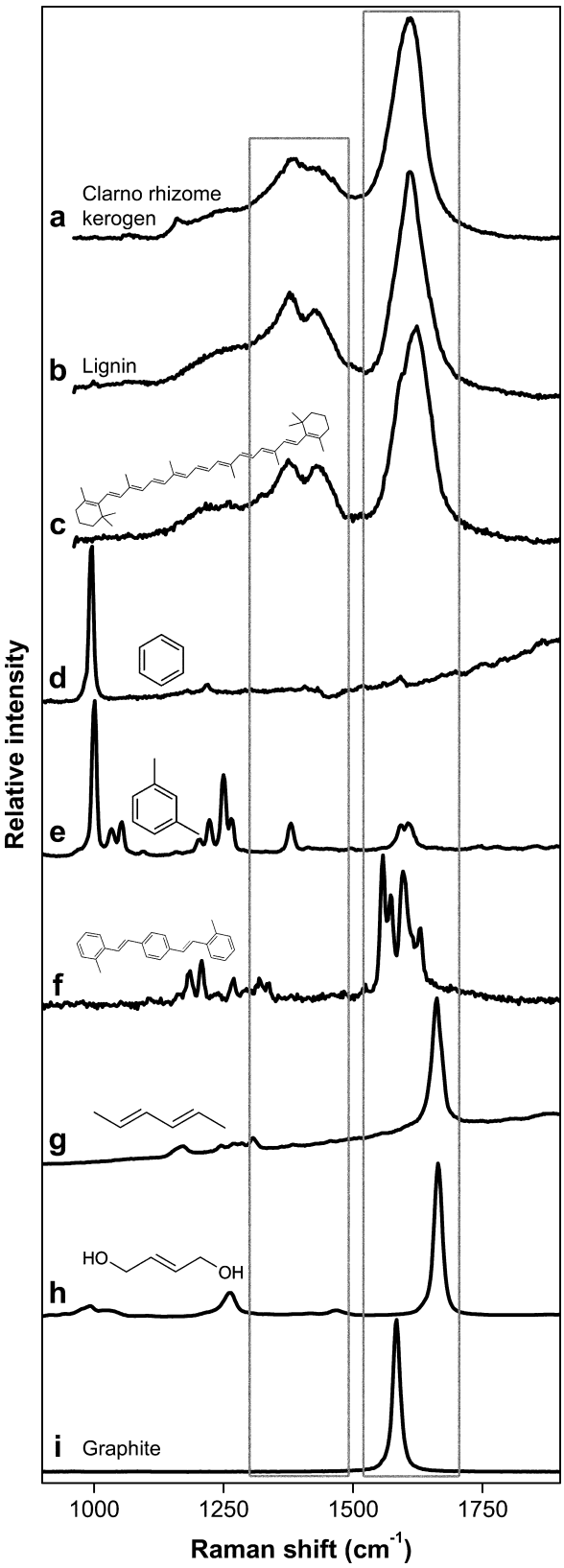

Fig. 6. UV–Raman spectra of Clarno fossil fern kerogen (a) for comparison with enzyme lignin (b) and other compounds that contain structures similar to those present in the kerogens (c–i). The polyene chain of β-carotene (c), bridging six-membered carbon rings, is particularly similar to structures present in the fossil kerogens. Other spectra shown are those of benzene (d), xylene (e), 1,4-bis(2-methylstyryl)benzene (f), 2,4-hexadiene (g), 2-butene-1,4-diol (h) and graphite (i).

Assignment of polyene chains in the kerogens is further supported by the UV–Raman analysis of model compounds. These show that neither the pattern of bands in the spectra of the kerogens nor the prominent constituents of these spectra can be attributed to vibrational modes of small aromatic molecules such as benzene or xylene (cf. Fig. 6a with 6d and e). Similarly, the pattern of bands is not attributable to the vibrational modes of simple polyenes or to those of similar olefinic materials, though such compounds do exhibit bands in the ca. 1560 to 1670 cm^{-1} region (compare Fig. 6a with 6f–h). Graphite, a material composed entirely of fused aromatic rings, similarly has a band in the ca. 1600 cm^{-1} region (Fig. 6i), but exhibits a pattern that differs substantially from that of the fossil fern kerogen spectra.

We attribute the band centered at 1625 cm^{-1} in the UV–Raman spectra of the Clarno fossil ferns (Fig. 5) to C=C stretching of relatively short polyene chains (Saito et al., 1983; Lin-Vien et al., 1991). Two additional lines of evidence support this interpretation. First, the Raman bands produced by such vibrational modes are resonantly enhanced by short (UV) excitation wavelengths, whereas those produced by vibrational modes of longer chain polyenes are not (Saito et al., 1983). Second, the peak position of the polyene C=C stretching vibration is known to shift from lower to higher wavenumbers with decreasing chain length (Bianco et al., 2004). A weak band in the spectra of such fossils centered at ca. 1530 cm^{-1} (Fig. 5) may be ascribable to C=C stretching of longer chain polyenes (Saito et al., 1983; Bianco et al., 2004). We attribute the band centered at ca. 1595 cm^{-1} (Fig. 5) to the synchronous ring stretching vibration of PAHs (Mapelli et al., 1999; Ferrari and Robertson, 2001; Schopf et al., 2005), an interpretation consistent with the abundance of aromatic carbon in the fern kerogen and the similarity of the position of this band to that of the sole UV–Raman spectral band of graphite (Fig. 6i). In summary, the UV–Raman spectra are interpreted to contain evidence of both short and relatively long polyene chains interlinking small PAH moieties.

In contrast to the UV–Raman bands discussed above, those between 1100 and 1500 cm^{-1} (Fig. 5) are more difficult to assign. Peaks in this region can be produced by vibrational modes of disparate molecular structures (including C—H vibrations of —CH_3 and =CH_2 groups and ring breathing of aromatic structures in small PAHs; Lin-Vien et al., 1991; Ferrari and Robertson, 2001; Jackson et al., 2003). However, UV–Raman studies of amorphous carbon networks that have spectra similar to those of the fossil ferns demonstrate that the bands in the 1100–1500 cm^{-1} region are not a result of C—H vibrations (Ferrari and Robertson, 2001; Chua and Stair, 2003; Jackson et al., 2003). Further, the similarity of these bands to those in materials that lack PAH moieties (discussed above) indicates that PAH ring breathing is unlikely to be the source. Rather, bands in the 1100 to 1500 cm^{-1} region of the UV–Raman spectra of the Clarno rhizomes seem more plausibly attributable to vibrational modes of C=C bonds in polyenes (the identity of which we have not yet firmly determined, though vibrational stretching modes of the double bonds in polyene chains, at ca. 1370 and 1430 cm^{-1}, correspond to two such positions; Inagaki et al., 1975).

The final region of interest in the UV–Raman spectra of the fossil ferns is that at 1700–1800 cm^{-1}. A small spectral shoulder is centered at ca. 1760 cm^{-1} (indicated by the arrow in Fig. 5) in all the spectra of kerogen of the Clarno and Princeton fossil ferns and is attributed to C=O stretching (Lin-Vien et al., 1991; Schopf et al., 2005). This interpretation is consistent with results obtained from py–GC–MS and ^{13}C NMR that demonstrate the presence of such carbonyl groups. Such structures have been proposed to be parts of bridging groups between the aromatic constituents of kerogen (Behar and Vandenbroucke, 1987; Siskin and Katritzky, 1991).

3.2.2. Rhizomes of the Clarno and Princeton cherts

The UV–Raman-detectable structures of the fern kerogens are very similar to each other. The only significant difference is the intensity of the bands in the ca. 1400 cm^{-1} region relative to those in the ca. 1600 cm^{-1} region (Fig. 7a). However, because the bands in the ca. 1400 cm^{-1} region have not been firmly identified, the structural basis for this spectral difference has yet to be determined.

Though similar to one another in overall composition, fern kerogens of the two cherts differ appreciably in the relative proportions of their molecular constituents. The Clarno kerogen contains a greater proportion of aromatic carbon and a smaller proportion of aliphatic carbon (predominantly in the form of C_{12} to C_{24} alkane and alkene chains; Figs. 3, 7b and c, and Table 2). Additionally, the Clarno kerogen exhibits a smaller proportion of oxygen-substituted carbon (Fig. 7b and Table 2). Such differences indicate that the fossil ferns of the Clarno chert, though well preserved, are more altered than those of the Princeton chert.

Although, overall, the amount of oxygen-substitution is less in the kerogen from fern specimens of the Clarno chert than from those of the Princeton chert, kerogens of the two units differ with regard to the types of carbon to which oxygen is bound. Compared to the Princeton kerogen, that of the Clarno contains a smaller proportion of oxygen bound to aromatic carbon, but a larger proportion of carboxyl carbon (Fig. 7c). Because the Clarno chert contains appreciably less OM than the Princeton chert (see Section 3.1) and exhibits a relatively higher degree of aromaticity (see above), the larger proportion of carboxyl groups in the Clarno kerogen may be a product of oxidation during diagenesis rather than a reflection of original biochemistry. As reported by Riboulleau et al. (2001) and Vandenbroucke and Largeau (2007), such oxidation of preserved OM typically results in a decrease in total organic carbon and an increase in the kerogen oxygen/carbon ratio by cross-linking of aromatic and aliphatic subunits with ester bonds. That the overall oxygen content of the Clarno fern kerogen is not greater than that of the Princeton specimens suggests that aromatic-bound oxygen was lost prior to carboxyl-producing diagenesis.

The timing of such carboxyl-producing oxidation can be constrained, at least in part, by analysis of the morphology of the preserved fossils. Optical microscopy shows that, prior to permineralization, fungi had infested virtually all of the fern axes of the Princeton chert (Fig. 1b) and some of those of the Clarno chert. Because fungi are obligate aerobes, the sediments in which the infested ferns were buried could not have been anoxic. However, the exceptional cellular preservation of all of the fossils (e.g., Fig. 1) indicates that the fern axes of both units were permineralized relatively rapidly. Thus, the short duration of oxidizing conditions prior to permineralization suggests that the carboxyl-producing oxidation must have occurred some time later, perhaps caused by groundwater percolating through the two units.

4. Conclusions

Analysis using UV–Raman (used here for the first time to investigate permineralized fossils), in combination with py–GC–MS and ^{13}C NMR, indicates that the kerogens of the fossil ferns are composed of networks of aromatic rings, small PAHs, aliphatic chains and short polyene chains. In addition, the study demonstrates that in such kerogens, polyenes, having resonantly enhanced UV–Raman spectral bands, can be detected in trace amounts. Future work will include Raman analyses using multiple ultraviolet laser lines, which, because of the wavelength dependence of the relative intensities of resonantly enhanced Raman bands, will allow us to further investigate the identities of the various structural components of these kerogens.

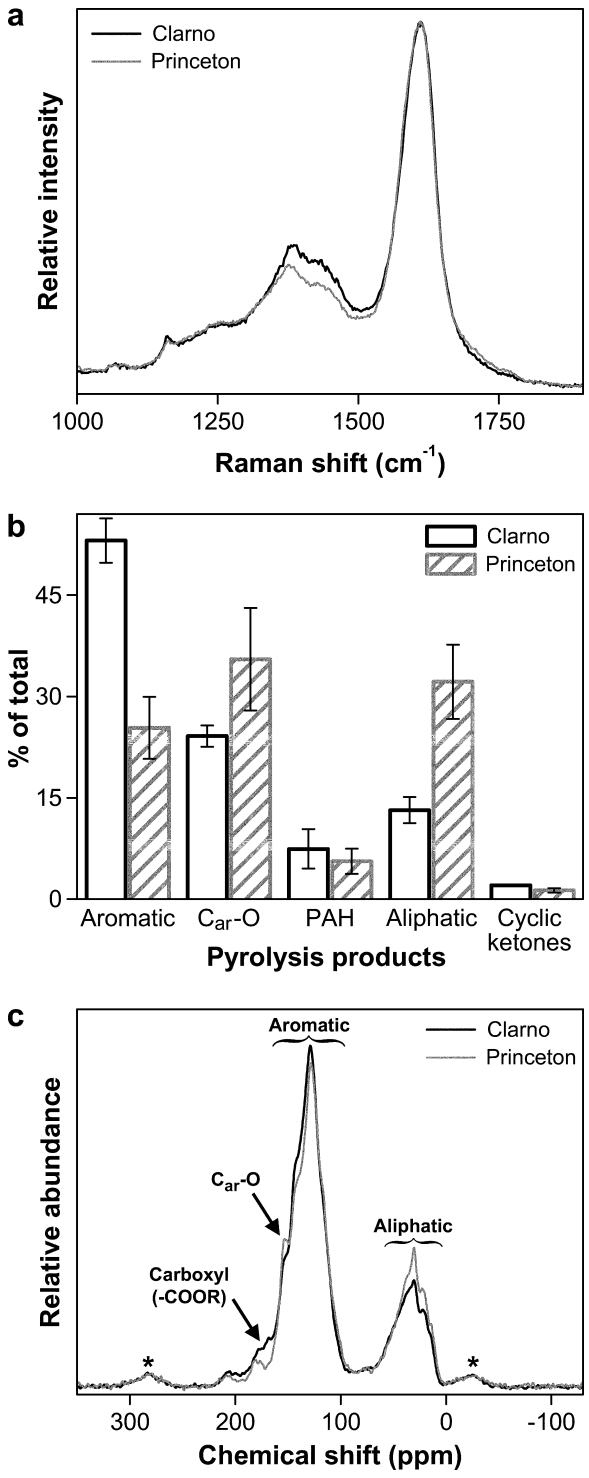

Fig. 7. Comparison of the fern kerogens permineralized in the Clarno and Princeton cherts. (a) Representative UV–Raman spectra of fern xylem cell walls preserved in each of the geologic units. (b) Average abundances of the macromolecular constituents of the kerogens of each unit (ratios of the sum of measured areas of the individual peaks in each pyrolysis product category [see Table 2] to those of the total ion chromatograms expressed as percentages; Clarno, $n = 2$; Princeton, $n = 3$; error bars are ±1 standard deviation). (c) Representative ^{13}C NMR spectra of kerogen from each unit, normalized by area; asterisks denote spinning side bands of main aromatic carbon band at ca. 130 ppm; assignment of labeled bands is discussed in the text.

The cellularly preserved fossil ferns are members of a single taxon permineralized in cherts of the Eocene Clarno and Allenby Formations, two units of essentially identical mineralogy and geologic

age. Despite these similarities, fossils from the two units are preserved somewhat differently. In each unit, the kerogenous OM is composed largely of interlinked aromatic and aliphatic compounds, but the kerogen of the Clarno chert is demonstrably more mature, i.e. more geochemically altered, than that of the Princeton chert. The differences in the composition of the kerogens in the two units are interpreted to be a result of differing post-permineralization geologic history. Studies such as this, combined with previous investigations of permineralized fossils preserved in rocks that are appreciably more altered than the essentially unmetamorphosed cherts studied here (Schopf et al., 2005), can be expected to provide important new insights into the geochemical changes in preserved OM that occur in pre-metamorphic geologic terrains.

Acknowledgements

The research was supported by NASA Exobiology Grant NAG5-12357 to J.W.S., the IGPP Center for the Study of Evolution and the Origin of Life (CSEOL), and an NSF Pre-doctoral Fellowship, a CSEOL Fellowship, Sigma Xi Grants-in-Aid of Research and a Geological Society of America Student Research Grant to A.D.C. Samples of the Princeton chert were provided by R. Stockey, University of Alberta, Edmonton. For technical assistance, we thank R. Alkaly and E. Ruth. We also thank N. Gupta and D. Curry for helpful comments and suggestions.

Associate Editor—**K.E. Peters**

References

Allwood, A.C., Walter, M.R., Marshall, C.P., 2006. Raman spectroscopy reveals thermal palaeoenvironments of c. 3.5 billion-year-old organic matter. Vibrational Spectroscopy 41, 190–197.

Almendros, G., Zancada, M.C., Gonzalez-Vila, F.J., Lesiak, M.A., Alvarez-Ramis, C., 2005. Molecular features of fossil organic matter in remains of the Lower Cretaceous fern *Weichselia reticulata* from Przenosza basement (Poland). Organic Geochemistry 36, 1108–1115.

Arnold, C.A., Daugherty, L.H., 1964. A fossil dennstaedtioid fern from the Eocene Clarno Formation of Oregon. Contributions from the Museum of Paleontology, University of Michigan 19, 65–88.

Arouri, K.R., Greenwood, P.F., Walter, M.R., 2000. Biological affinities of Neoproterozoic acritarchs from Australia: microscopic and chemical characterisation. Organic Geochemistry 31, 75–89.

Asher, S.A., 1984. Ultraviolet resonance Raman spectrometry for detection and speciation of trace polycyclic aromatic hydrocarbons. Analytical Chemistry 56, 720–724.

Asher, S.A., 1993. UV resonance Raman spectroscopy for analytical, physical, and biophysical chemistry: part 2. Analytical Chemistry 65, 201A–210A.

Asher, S.A., Johnson, C.R., 1984. Raman spectroscopy of a coal liquid shows that fluorescence interference is minimized with ultraviolet excitation. Science 225, 311–313.

Axelson, D.E., 1985. Solid State Nuclear Magnetic Resonance of Fossil Fuels. Multiscience Publications Ltd., Canada.

Barańska, H., Łabudzińska, A., Terpiński, J., 1987. Laser Raman Spectrometry: Analytical Applications. Ellis Horwood Ltd., Chichester.

Behar, F., Vandenbroucke, M., 1987. Chemical modelling of kerogens. Organic Geochemistry 11, 15–24.

Bernard, S., Benzerara, K., Beyssac, O., Menguy, N., Guyot, F., Brown, G.E., Goffe, B., 2007. Exceptional preservation of fossil plant spores in high-pressure metamorphic rocks. Earth and Planetary Science Letters 262, 257–272.

Beyssac, O., Goffé, B., Chopin, C., Rouzaud, J.N., 2002. Raman spectra of carbonaceous material in metasediments: a new geothermometer. Journal of Metamorphic Geology 20, 859–871.

Bianco, A., Del Zoppo, M., Zerbi, G., 2004. Experimental CC stretching phonon dispersion curves and electron phonon coupling in polyene derivatives. Journal of Chemical Physics 120, 1450–1457.

Boyce, C.K., Cody, G.D., Feser, M., Jacobsen, C., Knoll, A.H., Wirick, S., 2002. Organic chemical differentiation within fossil plant cell walls detected with X-ray spectromicroscopy. Geology 30, 1039–1042.

Boyce, C.K., Cody, G.D., Fogel, M.L., Hazen, R.M., Alexander, C.M.O.D., Knoll, A.H., 2003. Chemical evidence for cell wall lignification and the evolution of tracheids in early Devonian plants. International Journal of Plant Sciences 164, 691–702.

Boyce, C.K., Hotton, C.L., Fogel, M.L., Cody, G.D., Hazen, R.M., Knoll, A.H., 2007. Devonian landscape heterogeneity recorded by a giant fungus. Geology 35, 399–402.

Briggs, D.E.G., 1999. Molecular taphonomy of animal and plant cuticles: selective preservation and diagenesis. Philosophical Transactions of the Royal Society B: Biological Sciences 354, 7–17.

Briggs, D.E.G., Stankiewicz, B.A., Meischner, D., Bierstedt, A., Evershed, R.P., 1998. Taphonomy of arthropod cuticles from Pliocene lake sediments, Willershausen, Germany. Palaios 13, 386–394.

Bustin, R.M., Link, C., Goodarzi, F., 1989. Optical properties and chemistry of graptolite periderm following laboratory simulated maturation. Organic Geochemistry 14, 355–364.

Cevallos-Ferriz, S.R.S., Stockey, R.A., Pigg, K.B., 1991. The Princeton chert: evidence for *in situ* aquatic plants. Review of Palaeobotany and Palynology 70, 173–185.

Chen, J.-Y., Schopf, J.W., Bottjer, D.J., Zhang, C.-Y., Kudryavtsev, A.B., Tripathi, A.B., Wang, X.-Q., Yang, Y.-H., Gao, X., Yang, Y., 2007. Raman spectra of a Lower Cambrian ctenophore embryo from southwestern Shaanxi, China. Proceedings of the National Academy of Sciences of the USA 104, 6289–6292.

Chua, Y.T., Stair, P.C., 2003. An ultraviolet Raman spectroscopic study of coke formation in methanol to hydrocarbons conversion over zeolite H-MFI. Journal of Catalysis 213, 39–46.

Cody, G.D., Alexander, C.M.O., Tera, F., 2002. Solid-state (^{1}H and ^{13}C) nuclear magnetic resonance spectroscopy of insoluble organic residue in the Murchison meteorite: a self-consistent quantitative analysis. Geochimica et Cosmochimica Acta 66, 1851–1865.

Cody, G.D., Sághi-Szabó, G., 1999. Calculation of the ^{13}C NMR chemical shift of ether linkages in lignin derived geopolymers: constraints on the preservation of lignin primary structure with diagenesis. Geochimica et Cosmochimica Acta 63, 193–205.

Czaja, A.D., 2006. Characterization of the Geochemical Alteration of Permineralized Fossil Plants Based on Macromolecular Structure and Composition. Ph.D. Thesis, University of California, Los Angeles, Los Angeles, USA.

Czaja, A.D., Kudryavtsev, A.B., Schopf, J.W., 2006. New method for the microscopic, nondestructive acquisition of ultraviolet resonance Raman spectra from plant cell walls. Applied Spectroscopy 60, 352–355.

de Leeuw, J.W., Largeau, C., 1993. A review of macromolecular organic compounds that comprise living organisms and their role in kerogen, coal, and petroleum formation. In: Engel, M.H., Mako, S.A. (Eds.), Organic Geochemistry. Plenum, New York, pp. 23–72.

Dietrich, D., Witke, K., Röbler, R., Marx, G., 2001. Raman spectroscopy on *Psaronius* sp: a contribution to the understanding of the permineralization process. Applied Surface Science 179, 230–233.

Dutta, S., Brocke, R., Hartkopf-Fröder, C., Littke, R., Wilkes, H., Mann, U., 2007. Highly aromatic character of biogeomacromolecules in Chitinozoa: a spectroscopic and pyrolytic study. Organic Geochemistry 38, 1625–1642.

Faix, O., Meier, D., Fortmann, I., 1990. Thermal degradation products of wood gas chromatographic separation and mass spectrometric characterization of monomeric lignin derived products. Holz als Roh-und Werkstoff 48, 281–285.

Ferrari, A.C., Robertson, J., 2001. Resonant Raman spectroscopy of disordered, amorphous, and diamond like carbon. Physical Review B 64, 075414.

Gil, A.M., Neto, C.P., 1999. Solid-state NMR studies of wood and other lignocellulosic materials. Annual Reports on NMR Spectroscopy 37, 75–117.

Gilkes, K.W.R., Sands, H.S., Batchelder, D.N., Milne, W.I., Robertson, J., 1998. Direct observation of sp^3 bonding in tetrahedral amorphous carbon UV Raman spectroscopy. Journal of Non-Crystalline Solids, 612–616.

Greenwood, P.F., George, S.C., Pickel, W., Yangming, Z., Ningning, Z., 2001. In situ analytical pyrolysis of coal macerals and solid bitumens by laser micropyrolysis GC–MS. Journal of Analytical and Applied Pyrolysis, 237–253.

Greenwood, P.F., George, S.C., Wilson, M.A., Hall, K.J., 1996. A new apparatus for laser micropyrolysis–gas chromatography/mass spectrometry. Journal of Analytical and Applied Pyrolysis 38, 101–118.

Greenwood, P.F., van Heemst, J.D.H., Guthrie, E.A., Hatcher, P.G., 2002. Laser micropyrolysis GC–MS of lignin. Journal of Analytical and Applied Pyrolysis 62, 365–373.

Greenwood, P.F., Zhang, E., Vastola, F.J., Hatcher, P.G., 1993. Laser micropyrolysis–gas chromatography/mass spectrometry of coal. Analytical Chemistry 65, 1937–1946.

Gupta, N.S., Briggs, D.E.G., Collinson, M.E., Evershed, R.P., Michels, R., Jack, K.S., Pancost, R.D., 2007a. Evidence for the in situ polymerisation of labile aliphatic organic compounds during the preservation of fossil leaves: implications for organic matter preservation. Organic Geochemistry 38, 499–522.

Gupta, N.S., Briggs, D.E.G., Collinson, M.E., Evershed, R.P., Michels, R., Pancost, R.D., 2007b. Molecular preservation of plant and insect cuticles from the Oligocene Enspel Formation, Germany: evidence against derivation of aliphatic polymer from sediment. Organic Geochemistry 38, 404–418.

Gupta, N.S., Briggs, D.E.G., Landman, N.H., Tanabe, K., Summons, R.E., 2008a. Molecular structure of organic components in cephalopods: evidence for oxidative cross linking in fossil marine invertebrates. Organic Geochemistry 39, 1405–1414.

Gupta, N.S., Briggs, D.E.G., Pancost, R.D., 2006a. Molecular taphonomy of graptolites. Journal of the Geological Society, London 163, 897–900.

Gupta, N.S., Cambra-Moo, O., Briggs, D.E.G., Love, G.D., Fregenal-Martinez, M.A., Summons, R.E., 2008b. Molecular taphonomy of macrofossils from the Cretaceous Las Hoyas Formation, Spain. Cretaceous Research 29, 1–8.

Gupta, N.S., Collinson, M.E., Briggs, D.E.G., Evershed, R.P., Pancost, R.D., 2006b. Reinvestigation of the occurrence of cutan in plants: implications for the leaf fossil record. Paleobiology 32, 432–449.

Gupta, N.S., Michels, R., Briggs, D.E.G., Collinson, M.E., Evershed, R.P., Pancost, R.D., 2007c. Experimental evidence for the formation of geomacromolecules from plant leaf lipids. Organic Geochemistry 38, 28–36.

Gupta, N.S., Michels, R., Briggs, D.E.G., Evershed, R.P., Pancost, R.D., 2006c. The organic preservation of fossil arthropods: an experimental study. Proceedings of the Royal Society B, Biological Sciences 273, 2777–2783.

Gupta, N.S., Tetlie, O.E., Briggs, D.E.G., Pancost, R.D., 2007d. The fossilization of eurypterids: a result of molecular transformations. Palaios 22, 439–447.

Halttunen, M., Vyörykkä, J., Hortling, B., Tamminen, T., Batchelder, D., Zimmermann, A., Vuorinen, T., 2001. Study of residual lignin in pulp by UV resonance Raman spectroscopy. Holzforschung 55, 631–638.

Hatcher, P.G., Lerch III, H.E., Kotra, R.K., Verheyen, T.V., 1988. Pyrolysis g.c.-m.s. of a series of degraded woods and coalified logs that increase in rank from peat to subbituminous coal. Fuel 67, 1069–1075.

Hemsley, A.R., Barrie, P.J., Scott, A.C., 1995. ^{13}C solid-state NMR spectroscopy of fossil sporopollenins: variation in composition independent of diagenesis. Fuel 74, 1009–1012.

Hemsley, A.R., Scott, A.C., Barrie, P.J., Chaloner, W.G., 1996. Studies of fossil and modern spore wall biomacromolecules using ^{13}C solid state NMR. Annals of Botany 78, 83–94.

Hunt, J.M., 1996. Petroleum Geochemistry and Geology, 2nd ed. W.H. Freeman and Company, New York.

Inagaki, F., Tasumi, M., Miyazawa, T., 1975. Vibrational analysis of polyene chains. Assignments of resonance Raman lines of poly(acetylene) and β-carotene. Journal of Raman Spectroscopy 3, 335–343.

Ishiwatari, R., Ishiwatari, M., Kaplan, I.R., Rohrback, B.G., 1976. Thermal alteration of young kerogen in relation to petroleum genesis. Nature 264, 347–349.

Ishiwatari, R., Ishiwatari, M., Rohrback, B.G., Kaplan, I.R., 1977. Thermal alteration experiments on organic matter from recent marine sediments in relation to petroleum genesis. Geochimica et Cosmochimica Acta 41, 815–828.

Jackson, B.R., Trout, C.C., Badding, J.V., 2003. UV Raman analysis of the C:H network formed by compression of benzene. Chemistry of Materials 15, 1820–1824.

Jacob, J., Paris, F., Monod, O., Miller, M.A., Tang, P., George, S.C., Bény, J.M., 2007. New insights into the chemical composition of chitinozoans. Organic Geochemistry 38, 1782–1788.

Jehlička, J., Beny, C., 1999. First and second order Raman spectra of natural highly carbonified organic compounds from metamorphic rocks. Journal of Molecular Structure, 541–545.

Kingma, K.J., Hemley, R.J., 1994. Raman spectroscopic study of microcrystalline silica. American Mineralogist 79, 269–273.

Kiyokawa, S., Ito, T., Ikehara, M., Kitajima, F., 2006. Middle Archean volcano-hydrothermal sequence: bacterial microfossil-bearing 3.2 Ga Dixon Island Formation, coastal Pilbara terrane, Australia. Geological Society of America Bulletin 118, 3–22.

Kudryavtsev, A.B., Schopf, J.W., Agresti, D.G., Wdowiak, T.J., 2001. *In situ* laser-Raman imagery of Precambrian microscopic fossils. Proceedings of the National Academy of Sciences of the USA 98, 823–826.

Leary, G.J., Newman, R.H., 1992. Cross polarization/magic angle spinning nuclear magnetic resonance (CP/MAS NMR) spectroscopy. In: Lin, S.Y., Dence, C.W. (Eds.), Methods in Lignin Chemistry. Springer-Verlag, Berlin, pp. 146–161.

Li, C., Stair, P.C., 1997. Coke formation in zeolites studied by a new technique: ultraviolet resonance Raman spectroscopy. In: Progress in Zeolite and Microporous Materials, Pt. A, vol. 105. Studies in Surface Science and Catalysis. Elsevier Science B.V., pp. 599–606.

Li, C., Stair, P.C., 1997b. Ultraviolet Raman spectroscopy characterization of coke formation in zeolites. Catalysis Today 33, 353–360.

Lin-Vien, D., Colthup, N.B., Fateley, W.G., Grasselli, J.G., 1991. The Handbook of Infrared and Raman Characteristic Frequencies of Organic Molecules. Academic Press, Inc., Boston.

Lyons, P.C., Orem, W.H., Mastalerz, M., Zodrow, E.L., Vieth-Redemann, A., Bustin, R.M., 1995. ^{13}C NMR, micro-FTIR and fluorescence spectra, and pyrolysis–gas chromatograms of coalified foliage of late Carboniferous medullosan seed ferns, Nova Scotia, Canada: implications for coalification and chemotaxonomy. International Journal of Coal Geology 27, 227–248.

Mapelli, C., Castiglioni, C., Zerbi, G., 1999. Common force field for graphite and polycyclic aromatic hydrocarbons. Physical Review B 60, 12710–12725.

Marshall, C.P., Javaux, E.J., Knoll, A.H., Walter, M.R., 2005a. Combined micro-Fourier transform infrared (FTIR) spectroscopy and micro-Raman spectroscopy of Proterozoic acritarchs: a new approach to Palaeobiology. Precambrian Research 138, 208–224.

Marshall, C.P., Kannangara, G.S.K., Alvarez, R., Wilson, M.A., 2005b. Characterisation of insoluble charcoal in Weipa bauxite. Carbon 43, 1279–1285.

Marshall, C.P., Love, G.D., Snape, C.E., Hill, A.C., Allwood, A.C., Walter, M.R., Van Kranendonk, M.J., Bowden, S.A., Sylva, S.P., Summons, R.E., 2007. Structural characterization of kerogen in 3. 4 Ga Archaean cherts from the Pilbara Craton, Western Australia. Precambrian Research 155, 1–23.

Marshall, C.P., Mar, G.L., Nicoll, R.S., Wilson, M.A., 2001. Organic geochemistry of artificially matured conodonts. Organic Geochemistry 32, 1055–1071.

McKeegan, K.D., Kudryavtsev, A.B., Schopf, J.W., 2007. Raman and ion microscopic imagery of graphitic inclusions in apatite from older than 3830 Ma Akilia supracrustal rocks, west Greenland. Geology 35, 591–594.

Miller Jr., C.N., 1973. Silicified cones and vegetative remains of *Pinus* from the Eocene of British Columbia. Contributions from the Museum of Paleontology, University of Michigan 24, 101–118.

Nestler, K., Dietrich, D., Witke, K., Röβler, R., Marx, G., 2003. Thermogravimetric and Raman spectroscopic investigations on different coals in comparison to dispersed anthracite found in permineralized tree fern *Psaronius* sp. Journal of Molecular Structure, 357–362.

Pasteris, J.D., Wopenka, B., 1991. Raman spectra of graphite as indicators of degree of metamorphism. The Canadian Mineralogist 29, 1–9.

Pastorova, I., Botto, R.E., Arisz, P.W., Boon, J.J., 1994. Cellulose char structure: a combined analytical Py–GC–MS, FTIR, and NMR study. Carbohydrate Research 262, 27–47.

Peters, K.E., Ishiwatari, R., Kaplan, I.R., 1977. Color of kerogen as index of organic maturity. The American Association of Petroleum Geologists Bulletin 61, 504–510.

Pouwels, A.D., Eijkel, G.B., Boon, J.J., 1989. Curie-point pyrolysis capillary gas chromatography high-resolution mass–spectrometry of microcrystalline cellulose. Journal of Analytical and Applied Pyrolysis 14, 237–280.

Ralph, J., Hatfield, R.D., 1991. Pyrolysis–GC–MS characterization of forage materials. Journal of Agricultural and Food Chemistry 39, 1426–1437.

Riboulleau, A., Derenne, S., Largeau, C., Baudin, F., 2001. Origin of contrasting features and preservation pathways in kerogens from the Kashpir oil shales (Upper Jurassic, Russian Platform). Organic Geochemistry 32, 647–665.

Roberts, S., Tricker, P.M., Marshall, J.E.A., 1995. Raman spectroscopy of chitinozoans as a maturation indicator. Organic Geochemistry 23, 223–228.

Rullkötter, J., Michaelis, W., 1990. The structure of kerogen and related materials. A review of recent progress and future trends. Organic Geochemistry 16, 829–852.

Saito, S., Tasumi, M., Eugster, C.H., 1983. Resonance Raman spectra (5800–40 cm^{-1}) of all-*trans* and 15-*cis* isomers of β-carotene in the solid state and in solution. Measurements with various laser lines from ultraviolet to red. Journal of Raman Spectroscopy 14, 299–309.

Schopf, J.W., Kudryavtsev, A.B., 2005. Three-dimensional Raman imagery of Precambrian microscopic organisms. Geobiology 3, 1–12.

Schopf, J.W., Kudryavtsev, A.B., Agresti, D.G., Czaja, A.D., Wdowiak, T.J., 2005. Raman imagery: a new approach to assess the geochemical maturity and biogenicity of permineralized Precambrian fossils. Astrobiology 5, 333–371.

Schopf, J.W., Kudryavtsev, A.B., Agresti, D.G., Wdowiak, T.J., Czaja, A.D., 2002. Laser-Raman imagery of Earth's earliest fossils. Nature 416, 73–76.

Schopf, J.W., Kudryavtsev, A.B., Czaja, A.D., Tripathi, A.B., 2007. Evidence of Archean life: stromatolites and microfossils. Precambrian Research 158, 141–155.

Schopf, J.W., Tewari, V.C., Kudryavtsev, A.B., 2008. Discovery of a new chert-permineralized microbiota in the Proterozoic Buxa Formation of the Ranjit Window, Sikkim, Northeast India, and its astrobiological implications. Astrobiology 8, 735–746.

Schweitzer, M.H., Marshall, M., Carron, K., Bohle, D.S., Busse, S.C., Arnold, E.V., Barnard, D., Horner, J.R., Starkey, J.R., 1997. Heme compounds in dinosaur trabecular bone. Proceedings of the National Academy of Sciences of the USA 94, 6291–6296.

Siskin, M., Katritzky, A.R., 1991. Reactivity of organic compounds in hot water: geochemical and technological implications. Science 254, 231–237.

Smith, S.Y., Stockey, R.A., 2003. Aroid seeds from the Middle Eocene Princeton chert (*Keratosperma allenbyense*, Araceae): comparisons with extant Lasioideae. International Journal of Plant Science 164, 239–250.

Snape, C.E., Ladner, W.R., Bartle, K.D., 1979. Survey of ^{13}C chemical shifts in aromatic hydrocarbons and its application to coal-derived materials. Analytical Chemistry 51, 2189–2198.

Stankiewicz, B.A., Briggs, D.E.G., Michels, R., Collinson, M.E., Flannery, M.B., Evershed, R.P., 2000. Alternative origin of aliphatic polymer in kerogen. Geology 28, 559–562.

Stankiewicz, B.A., Kruge, M.A., Mastalerz, M., Salmon, G.L., 1996. Geochemistry of the alginate and amorphous organic matter from Type II-S kerogens. Organic Geochemistry 24, 495–509.

Stankiewicz, B.A., Mastalerz, M., Kruge, M.A., van Bergen, P.F., Sadowska, A., 1997. A comparative study of modern and fossil cone scales and seeds of conifers: a geochemical approach. New Phytologist 135, 375–393.

Stankiewicz, B.A., Scott, A.C., Collinson, M.E., Finch, P., Mösle, B., Briggs, D.E.G., Evershed, R.P., 1998. Molecular taphonomy of arthropod and plant cuticles from the Carboniferous of North America: implications for the origin of kerogen. Journal of the Geological Society, London 155, 453–462.

Sugitani, K., Grey, K., Allwood, A., Nagaoka, T., Mimura, K., Minami, M., Marshall, C.P., Van Kranendonk, M.J., Walter, M.R., 2007. Diverse microstructures from Archaean chert from the Mount Goldsworthy-Mount Grant area, Pilbara Craton, Western Australia: microfossils, dubiofossils, or pseudofossils? Precambrian Research 158, 228–262.

Tegelaar, E.W., de Leeuw, J.W., Derenne, S., Largeau, C., 1989. A reappraisal of kerogen formation. Geochimica et Cosmochimica Acta 53, 3103–3106.

Tissot, B.P., Welte, D.H., 1984. Petroleum Formation and Occurrence, 2nd ed. Springer-Verlag, Berlin.

Ueno, Y., Isozaki, Y., Yurimoto, H., Maruyama, S., 2001. Carbon isotopic signatures of individual Archean microfossils from Western Australia. International Geology Review 43, 196–212.

van Bergen, P.F., Collinson, M.E., Hatcher, P.G., de Leeuw, J.W., 1994a. Lithological control on the state of preservation of fossil seed coats of water plants. Organic Geochemistry 22, 683–702.

van Bergen, P.F., Hatcher, P.G., Boon, J.J., Collinson, M.E., de Leeuw, J.W., 1997. Macromolecular composition of the propagule wall of Nelumbo nucifera. Phytochemistry 45, 601–610.

van Bergen, P.F., Scott, A.C., Barrie, P.J., de Leeuw, J.W., Collinson, M.E., 1994b. The chemical composition of Upper Carboniferous pteridosperm cuticles. Organic Geochemistry 21, 107–112.

Vandenbroucke, M., Largeau, C., 2007. Kerogen origin, evolution and structure. Organic Geochemistry 38, 719–833.
VanderHart, D.L., Atalla, R.H., 1984. Studies of microstructure in native celluloses using solid-state ^{13}C NMR. Macromolecules 17, 1465–1472.
Walter, M.R., Hofmann, H.J., Schopf, J.W., 1983. Geographic and geologic data for processed rock samples. In: Schopf, J.W. (Ed.), Earth's Earliest Biosphere its Origin and Evolution. Princeton University Press, Princeton, NJ, pp. 385–413.
Wang, Y., Huang, Y.-S., Alexander, C.M.O., Fogel, M., Cody, G., 2005. Molecular and compound-specific hydrogen isotope analyses of insoluble organic matter from different carbonaceous chondrite groups. Geochimica et Cosmochimica Acta 69, 3711–3721.
Wellman, C.H., Axe, L., 1999. Extracting plant mesofossils and megafossils by bulk acid maceration. In: Jones, T.P., Rowe, N.P. (Eds.), Fossil Plants and Spores: Modern Techniques. Geological Society, London, pp. 11–14.
Wopenka, B., Pasteris, J.D., 1993. Structural characterization of kerogens to granulite-facies graphite: applicability of Raman microprobe spectroscopy. American Mineralogist 78, 533–557.
Yui, T.-F., Huang, E., Xu, J., 1996. Raman spectrum of carbonaceous material: a possible metamorphic grade indicator for low-grade metamorphic rocks. Journal of Metamorphic Geology 14, 115–124.
Yule, B., Roberts, S., Marshall, J.E.A., 2000. The thermal evolution of sporopollenin. Organic Geochemistry 31, 859–870.
Yule, B., Roberts, S., Marshall, J.E.A., Milton, J.A., 1998. Quantitative spore colour measurement using colour image analysis. Organic Geochemistry 28, 139–149.
Zang, W.L., 2007. Deposition and deformation of late Archaean sediments and preservation of microfossils in the Harris Greenstone Domain, Gawler Craton, South Australia. Precambrian Research 156, 107–124.